Development 138, 3179-3188 (2011) doi:10.1242/dev.058602

Bone morphogenetic proteins regulate neural tube closure by interacting with the apicobasal polarity pathway

Dae Seok Eom[1,2,*], Smita Amarnath[2], Jennifer L. Fogel[3,†] and Seema Agarwala[1,2,3,‡]

SUMMARY

During neural tube closure, specialized regions called hinge points (HPs) display dynamic and polarized cell behaviors necessary for converting the neural plate into a neural tube. The molecular bases of such cell behaviors (e.g. apical constriction, basal nuclear migration) are poorly understood. We have identified a two-dimensional canonical BMP activity gradient in the chick neural plate that results in low and temporally pulsed BMP activity at the ventral midline/median hinge point (MHP). Using in vivo manipulations, high-resolution imaging and biochemical analyses, we show that BMP attenuation is necessary and sufficient for MHP formation. Conversely, BMP overexpression abolishes MHP formation and prevents neural tube closure. We provide evidence that BMP modulation directs neural tube closure via the regulation of apicobasal polarity. First, BMP blockade produces partially polarized neural cells, which retain contact with the apical and basal surfaces but where basolateral proteins (LGL) become apically localized and apical junctional proteins (PAR3, ZO1) become targeted to endosomes. Second, direct LGL misexpression induces ectopic HPs identical to those produced by noggin or dominant-negative BMPR1A. Third, BMP-dependent biochemical interactions occur between the PAR3-PAR6-aPKC polarity complex and phosphorylated SMAD5 at apical junctions. Finally, partially polarized cells normally occur at the MHP, their frequencies inversely correlated with the BMP activity gradient in the neural plate. We propose that spatiotemporal modulation of the two-dimensional BMP gradient transiently alters cell polarity in targeted neuronal cells. This ensures that the neural plate is flexible enough to be focally bent and shaped into a neural tube, while retaining overall epithelial integrity.

KEY WORDS: Noggin, Hinge point, Apical constriction, Basal nuclear migration, Endocytosis, EEA1, RAB5, PAR3, Lethal giant larva, Tight junctions, Adherens junctions, Interkinetic nuclear migration, Midbrain, Chick

INTRODUCTION

During neurulation, a flat neural plate rolls up to form a closed neural tube. This process involves diverse cell behaviors at specialized regions of the neural plate called hinge points (HPs) (Davidson and Keller, 1999; Jacobson et al., 1986; Smith and Schoenwolf, 1997). At the ventral midline/median hinge point (MHP), polarized cell shape changes result in cells with reduced apical (apical constriction) and increased basal cell diameters (Colas and Schoenwolf, 2001). In association with the notochord, these cell shape changes buckle the ventral midline and elevate the neural folds. Subsequently, two dorsolateral hinge points (DLHPs) form, associate with the surface ectoderm, and push the neural folds together so that they fuse across the dorsal midline. Although the relative importance of the MHP and the DLHP differs across axial levels of the folding neural plate, together they play a key role in producing a closed neural tube with the correct cross-sectional morphology (Smith and Schoenwolf, 1997; Stottmann et al., 2006; Ybot-Gonzalez et al., 2002).

A role for cell cycle progression has been established in eliciting apicobasal shape changes at the MHP (Smith and Schoenwolf, 1987). As neural progenitors divide, they exhibit apicobasal (interkinetic) nuclear migration, always undergoing mitosis apically (Sauer, 1935). This has led to the idea that basal cell expansion at the MHP can be achieved simply by altering cell cycle progression so that nuclei are induced to remain basal, for example, by reducing mitotic duration and/or by increasing the duration of other cell cycle phases (Smith and Schoenwolf, 1987).

By contrast, recent studies implicate the active regulation of apical constriction in bending and shaping epithelial sheets, including the neural plate (Copp et al., 2003; Haigo et al., 2003; Nagele et al., 1989; Nishimura and Takeichi, 2008; Smith and Schoenwolf, 1997; van Straaten et al., 2002). This process requires contraction of the adherens belt, which runs immediately below the apical surface of epithelial sheets and can provide a mechanism for shaping whole tissues via its association with adherens junctions (Nishimura and Takeichi, 2008). Despite its importance in organogenesis, only a handful of molecules have been implicated in the regulation of apical constriction (Brouns et al., 2000; Haigo et al., 2003; Nishimura and Takeichi, 2008; Sai and Ladher, 2008).

How are the above apicobasal events (e.g. apical constriction, cell cycle progression, apicobasal span) regulated and coordinated during neural tube closure (Copp et al., 2003; Haigo et al., 2003; Nishimura and Takeichi, 2008; Yang et al., 2009)? Recently, the coordinated bending of epithelial sheets into complex organs has been attributed to the dynamic regulation of apicobasal epithelial polarity (Andrew and Ewald, 2010; Bryant and Mostov, 2008). According to these studies, simple epithelial sheets can progressively transform themselves into complex branched tubules by polarized cell divisions and the dynamic shunting of cells through unpolarized, semi-polarized and polarized states (Bryant and Mostov, 2008). In such 'morphogenetically active' epithelia, altering the polarity of a few cells at a time while retaining it in

[1]Institute for Cell and Molecular Biology, University of Texas at Austin, TX 78712, USA. [2]Section of Molecular, Cellular and Developmental Biology, University of Texas at Austin, Austin, TX 78713, USA. [3]Institute for Neuroscience, University of Texas at Austin, Austin, TX 78712, USA.

*Present address: Department of Biology, University of Washington, Seattle, WA 98195, USA
†Present address: Stem Cell and Regenerative Medicine, University of Southern California, Los Angeles, CA 90033, USA
‡Author for correspondence (agarwala@mail.utexas.edu)

Accepted 12 May 2011

others allows the epithelial sheet to retain its overall integrity while possessing the flexibility to be bent and shaped (Ewald et al., 2008; Yang et al., 2009).

Transforming growth factor beta (TGFβ) family members, including bone morphogenetic proteins (BMPs), have recently been implicated in epithelial tissue morphogenesis and have been shown to interact with tight and adherens junction proteins (Attisano and Wrana, 2002; Gibson and Perrimon, 2005; Shen and Dahmann, 2005; Shoval et al., 2007). For example, the disruption of tight junctions by TGFβ ligands has been shown to regulate epithelial-to-mesenchymal transformations, which frequently underlie tissue morphogenesis (Massague, 2008; Ozdamar et al., 2005). Furthermore, cadherin-mediated BMP activity is essential for neural crest migration and directional convergent extension movements, which narrow and elongate the fish embryo during gastrulation (Shoval et al., 2007; von der Hardt et al., 2007).

A role for BMP signaling in dorsal neural cell-fate specification is firmly established (Liu and Niswander, 2005). Interestingly, perturbed BMP signaling also results in neural tube closure defects, but little is known about the mechanisms underlying such defects (McMahon et al., 1998; Stottmann et al., 2006; Umans et al., 2003; Ybot-Gonzalez et al., 2007). In this study, we have examined the role of BMP signaling in closing the neural tube at the midbrain, a region where exencephaly occurs frequently, and where closure mechanisms are distinct from those employed in caudal neural tube (Copp et al., 2003). We show that a complex two-dimensional BMP gradient occurs in chick anterior neural plate and that its modulation profoundly affects MHP formation and midbrain neural tube closure. Using high-resolution imaging and biochemical analyses, we further demonstrate that BMP signal modulation dynamically regulates the early events of neural tube closure by interacting with members of the apicobasal polarity pathway.

MATERIALS AND METHODS

Chick embryos

Fertilized Leghorn eggs (Ideal Poultry, Cameron, TX, USA) were incubated at 38°C. Chick embryos were staged according to Hamburger and Hamilton (HH) (Hamburger and Hamilton, 1951).

Expression vectors

In vivo gene expression was driven by the pXex, pEFX, pMes or pCS2 expression vectors (Agarwala et al., 2001; Johnson and Krieg, 1994; Swartz et al., 2001). Embryos were electroporated with EGFP (Agarwala et al., 2001), membrane-targeted EGFP (mEGFP), noggin, dominant-negative BMP receptor 1A-IRES-EGFP (dnBMPR1A), constitutively active BMP receptor 1A-IRES-EGFP (caBMPR1A), LGL-GFP, PAR3-GFP and RAB5-mCherry.

In ovo electroporation

DNA (0.02-5 μg/μl) was electroporated into HH7-11 embryos, designated 'late' electroporations (Agarwala et al., 2001). For 'early' in vivo electroporations (HH4-6), the epiblast was irrigated with Ringer's solution and ~0.3 μl of DNA was injected into a lumen formed by the neural groove and the vitelline membrane. Embryos were micro-electroporated with the negative electrode placed in a pool of Ringer's on the vitelline membrane above the presumptive midbrain and the positive electrode positioned below the embryo (Agarwala et al., 2001; Colas and Schoenwolf, 2001). One in eight early electroporated embryos displayed morphological defects and were eliminated from analyses (Table 1).

In situ hybridization

Embryos were harvested between HH4 and embryonic day (E) 5 and immersion-fixed in 4% paraformaldehyde. One- or two-color in situ hybridizations were used to detect *BMP7*, *SHH*, chordin, noggin, *PHOX2A* and *PAX6* using established protocols (Agarwala and Ragsdale, 2002).

Immunohistochemistry

Embryos were fixed in 4% paraformaldehyde for 15 minutes to 2 hours. Transverse sections (14 μm) were stained with antibodies against pHH3 (Upstate; 1:500), PAR3 (Upstate; 1:500), phosphorylated (p) SMAD1/5/8 (Cell Signaling; 1:1000), N-cadherin (N-CAD; DSHB; 1:500), ZO-1 (BD Biosciences; 1:1000), EEA1 (BD Biosciences; 1:30), GFP (Molecular Probes; 1:500), SOX2 (Abcam; 1:250) and FOXA2, ISL1 and SHH (DSHB; all 1:250). Alexa Fluor-conjugated secondary antibodies were used for fluorescent detection (Afonso and Henrique, 2006). Alexa Fluor-conjugated phallotoxins (Molecular Probes) were used for F-actin detection. DAPI was used for staining nuclei.

Wholemount pSMAD1/5/8 immunohistochemistry

Wholemount pSMAD1/5/8 immunolabeling was conducted by adapting the wholemount in situ hybridization protocol described above, by substituting the probe hybridization step with a 2-day incubation in the primary antibody at 4°C (Agarwala and Ragsdale, 2002).

Imaging

Confocal images were obtained with a Zeiss laser scanning microscope (LSM5 Pascal) or an Olympus IX51 spinning disc microscope and captured with AxioVision (Zeiss) or Slidebook Pro (3I, CO, USA) software. Additional data analyses were conducted using Imaris software (Bitplane) and Photoshop (Adobe). Unless noted otherwise, confocal images are presented as single 0.5-0.8 μm optical sections.

Immunoprecipitation and western blot analysis

For western blotting, whole cell lysates were prepared from HH9-11 wild-type chick midbrains or the electroporated regions of E3 midbrains. Midbrain tissue was lysed with RIPA buffer (50 mM Tris pH 7.5, 150 mM NaCl, 0.1% SDS, 0.5% sodium deoxycholate, 1% Triton X-100, 1 mM PMSF) and loaded on a 12% SDS-PAGE gel. Protein (100 μg) from chick midbrains in HKET lysis buffer (25 mM HEPES pH 7.4, 150 mM NaCl, 1 mM EDTA, 1% Triton X-100, 100 mM DTT, protease inhibitor cocktail, 1 mM NaF, 0.1 mM sodium orthovanadate) was incubated with either 10 μg/ml normal rabbit IgG (Alpha Diagnostic International) or 20 μg/ml PAR3 (Millipore), aPKC (Santa Cruz Biotechnology), PAR6 (Abcam), SMAD1, SMAD5 or pSMAD1/5/8 (Cell Signaling Technology) antibodies. Protein complexes were immunoprecipitated using 20 μl Protein A/G agarose beads (Santa Cruz Biotechnology, CA, USA), separated by SDS-PAGE, immunoblotted with PAR3, pSMAD1/5/8, PAR6 or aPKC antibodies and detected by ECL chemiluminescence (Thermo Scientific). The molecular weights of PAR3, aPKC, PAR6, SMAD1, SMAD5 and pSMAD1/5/8 were ascertained using NCBI databases.

Quantitative analyses

Unless noted otherwise, all quantification was conducted using ImageJ software (NIH) on midbrains electroporated at HH4-6 and harvested at HH7. Quantitative data were obtained from two to three 14-μm sections per control or noggin-electroporated midbrain at its rostrocaudal midpoint. Data are displayed as the mean ± s.e.m.

Overlap between pSMAD1/5/8 and phospho-histone H3 (pHH3) expression

The overlap between mitotic ($pHH3^+$) and $pSMAD1/5/8^+$ cells was computed in HH7 midbrain transverse sections. All $pHH3^-$ $pSMAD1/5/8^+$ and $pHH3^+$ pSmad $1,5,8^+$ cells in two sections from each of five embryos were tabulated and expressed as a percentage of the total number of pSMAD $1/5/8^+$ cells. No $pHH3^+$ $pSMAD1/5/8^-$ cells were found in HH7 brains.

Apical constriction

Transverse sections obtained from embryos electroporated with mEGFP alone or mEGFP plus noggin were stained for the apical marker PAR3. The ratio of the apical width (aw) to the cell width at its widest point (ww, where the nucleus is invariably located) was computed as a measure of apical constriction according to established protocols (Lee et al., 2007). Only those $mEGFP^+$ cells for which entire outlines could be discerned in control (n=33 cells/6 embryos) and noggin-electroporated (n=41 cells/7

embryos) cells were included in these analyses. Differences in the aw:ww ratio between controls and noggin-electroporated embryos were evaluated using a *t*-test.

Basal nuclear migration

Basal nuclear migration was determined by centering a 70-μm × 70-μm sampling box in the lateral neural plate (controls) or at an ectopic HP in lateral neural plate (noggin-electroporated brains). A perpendicular line was drawn from the apical surface to the apical tip of each DAPI$^+$ cell in three sections per HH7 midbrain in control (n=5) and noggin-electroporated (n=6) embryos. The differences were evaluated using a *t*-test.

Apicobasal length

The apicobasal span of midbrain progenitors was measured in early HH7 brains electroporated with mEGFP alone or in conjunction with noggin. A sampling box was drawn on each of two sections positioned in the ventrolateral midbrain as above. Within the box, the apicobasal spans of all electroporated cells for which the outline could be fully visualized in control (n=17 cells/5 brains) and noggin-electroporated (n=42 cells/10 brains) brains were measured and compared using a *t*-test.

Apicobasal polarity

Embryos were electroporated with low-level LGL-GFP (1 μg/μl) between HH4-HH6 and examined at HH7 in transverse sections immunostained for GFP and PAR3. Unlike high-level LGL-GFP (3-5 μg/μl) electroporations, the low LGL-GFP concentration did not induce HPs or alter cell polarity in HH4-11 electroporations (Fig. 5C; Fig. 6C,E; see Fig. S6A,C in the supplementary material). Only those cells (n=35 cells/9 brains) with clearly discernible outlines were selected for analyses. Cells that displayed apical LGL-GFP, but maintained contact with the apical and basal surfaces, were designated as partially polarized (14/35 cells). Those cells that displayed full segregation between apical (PAR3$^+$) and basolateral (LGL-GFP$^+$) compartments were designated as polarized (27/35 cells).

The basal location of nuclei and apically condensed phalloidin identified the MHP (Colas and Schoenwolf, 2001). Cells located 50 μm or more from the MHP were designated as lateral. This region excluded the neural folds. The ratio of polarized to semi-polarized cells at the MHP (n=16 cells/7 midbrains) and lateral midbrain (n=19 cells/7 midbrains) were computed within a 70-μm × 70-μm sampling box. Similar data were obtained from the lateral midbrain of noggin-electroporated embryos (n=59 cells/6 midbrains). Pairwise comparisons were made using a *t*-test.

PAR3 endocytosis

z-stacks were collected from a 70-μm × 70-μm sampling box in control low LGL-GFP (n=72 cells/3 brains) and noggin plus low LGL-GFP (n=57 cells/3 brains) electroporated lateral midbrains stained for PAR3 and EEA1. The number of electroporated cells within the sampling box containing at least one PAR3$^+$ EEA1$^+$ punctum was compared with that in noggin plus low LGL-GFP electroporated brains (Bucci et al., 1992).

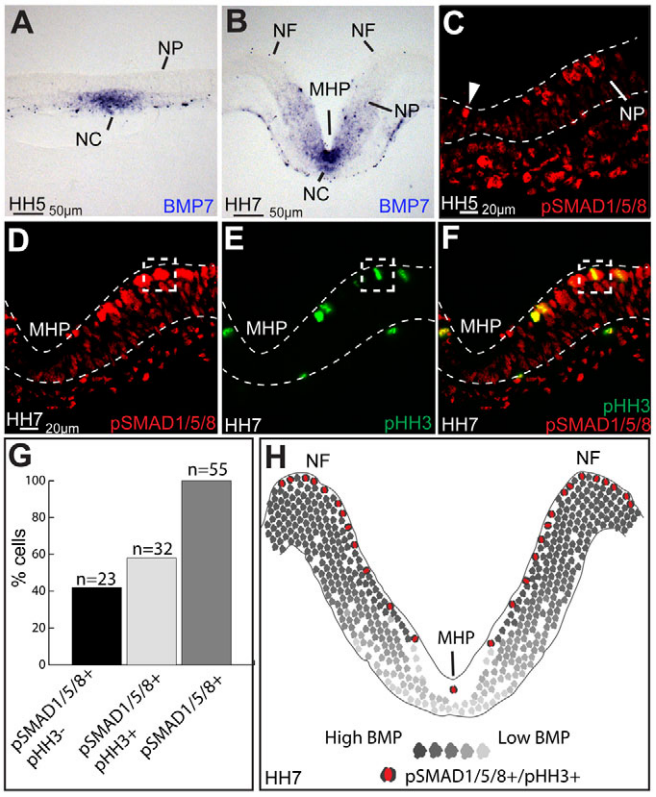

Fig. 1. BMP signaling in the folding neural plate. (**A**,**B**) *BMP7* mRNA expression in the chick notochord (NC) and the neural plate (NP). Embryonic stages are noted at the bottom left. NF, neural fold. (**C-F**) Neural plate hemi-sections showing lateromedially and apicobasally graded pSMAD1/5/8 expression (red). Note that only a few pSMAD1/5/8$^+$ cells (arrowhead, C) are present at the ventral midline/median hinge point (MHP) compared with lateral regions of the neural plate, making them difficult to visualize in transverse sections (C-F), but not in wholemounts (see Fig. S1G in the supplementary material). The colocalization of pSMAD1/5/8 with pHH3 (green) in apical mitotic cells is shown (e.g. boxed cell in D-F). The neural plate is outlined (dashed line). (**G**) Quantitation of pSMAD1/5/8 and pHH3 overlap in the neural plate. (**H**) Summary of data presented in A-G.

RESULTS

A two-dimensional, spatiotemporally dynamic BMP activity gradient in the neural plate

We examined BMP signaling in the neurulating chick embryo prior to (HH4-5) and during (HH6-7) MHP formation (Colas and Schoenwolf, 2001; Hamburger and Hamilton, 1951). *BMP7* expression was seen in the axial midline (e.g. notochord) by HH4-5 and in anterior notochord and the MHP by HH6-7 (Fig. 1A,B; see Fig. S1A,B in the supplementary material). However, BMP antagonists noggin and chordin were also simultaneously expressed along the axial midline of the chick at HH4-7 (see Fig. S1C-F in the supplementary material). To determine how these signals are integrated at the MHP, we examined the expression of phosphorylated (p) SMAD1/5/8, a definitive readout of canonical BMP signaling. Mosaic pSMAD1/5/8 labeling was seen at the apical surface of the presumptive neurectoderm at HH4-5 (Fig. 1C). By HH6-7, pSMAD1/5/8 expression occurred along two intersecting gradients in the neural plate (Fig. 1D; see Fig. S1G in the supplementary material). A lateromedial gradient of pSMAD1/5/8 expression was seen, with the lowest levels of expression at the MHP (Fig. 1D; see Fig. S1G in the supplementary material). A second pSMAD1/5/8 gradient was seen along the apicobasal (ventricular-pial) axis of the presumptive midbrain plate, with strong, but mosaic, expression in apical nuclei (Fig. 1D; see Fig. S1G in the supplementary material).

Neural progenitors undergo interkinetic nuclear migration as they progress through the cell cycle, with mitosis occurring apically (Sauer, 1935; Smith and Schoenwolf, 1997). Interestingly, 100% of pHH3$^+$ mitotic cells co-expressed high levels of pSMAD1/5/8 during neurulation, whereas 41% of apical pSMAD1/5/8$^+$ cells were pHH3$^-$ and presumably represented cells about to enter into mitosis or those that had just exited this phase (Fig. 1D-H) (Langman et al., 1966). Based on previous studies, neurulation stage neural progenitors exhibit a cell cycle of 7-12 hours, with 0.5-

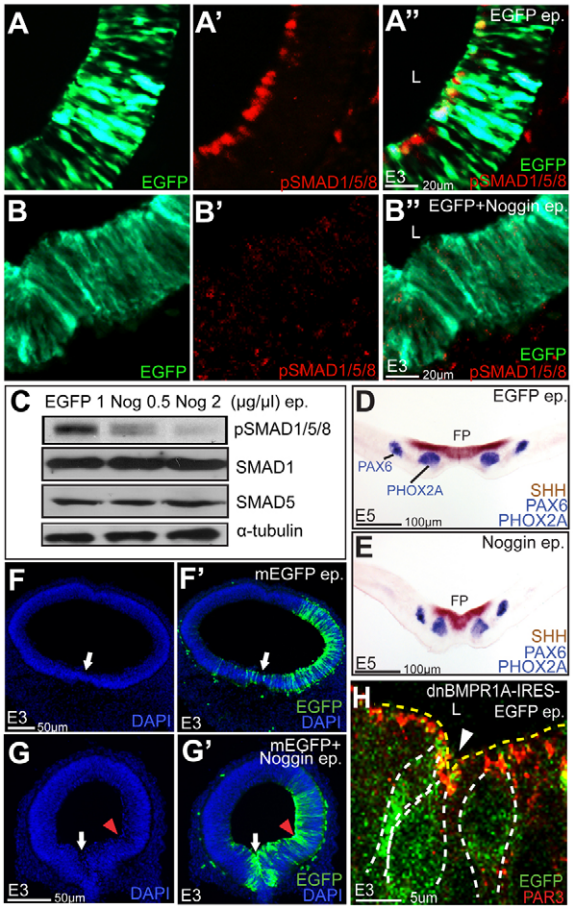

Fig. 2. BMP signaling regulates midbrain shape but not ventral cell-fate specification. (**A-B″**) Control (A-A″) and noggin (B-B″) electroporations (green cells) demonstrating severely reduced pSMAD1/5/8 (red) expression in the latter. L, lumen. (**C**) Western blots demonstrating that noggin reduces pSMAD1/5/8 levels in a dose-dependent manner, but does not change the absolute levels of SMAD1 or SMAD5 in E3 whole cell lysates. α-tubulin provides a loading control. (**D**,**E**) Control (D) and noggin-electroporated (E) midbrains demonstrating that ventral cell fates (expressing *SHH*, *PHOX2A* and *PAX6*) are not perturbed by BMP blockade. FP, floor plate. (**F-G′**) DAPI and EGFP staining of controls (F,F′) and noggin-electroporated brains (G,G′) demonstrating that noggin induces ectopic hinge-like invaginations (arrowhead) in lateral midbrain and exaggerated ventral midline grooving (arrow). (**H**) dnBMPR1A overexpression (green) in lateral midbrain also induces hinge-like invaginations (arrowhead) of the PAR3$^+$ (red) apical surface (arrowhead). The dashed yellow line delineates the apical surface, whereas the dashed white lines delineate the outlines of dnBMPR1A-electroporated cells.

1.3 hours allocated to mitosis (Schoenwolf, 1985; Smith and Schoenwolf, 1987). High BMP signaling is therefore received only transiently by apical mitotic progenitors during each cell cycle, with only a few pSMAD1/5/8$^+$ pHH3$^+$ cells present at the MHP compared with the rest of the neural plate (Fig. 1C-H). Together, these observations suggest that the MHP receives low levels of temporally dynamic canonical BMP signaling during neurulation (summarized in Fig. 1H).

BMP signaling regulates midbrain shape but not ventral cell-fate specification

We increased (caBMPR1A) or attenuated (noggin, dnBMPR1A) BMP signaling in the developing midbrain using in ovo electroporation. Immunohistochemical and western blot analyses following noggin electroporations (0.2-2 μg/μl) in the midbrain resulted in a dose-dependent reduction of pSMAD1/5/8 levels, but not in the total levels of SMAD1 or SMAD5 proteins (Fig. 2A-C). Since *BMP7* is co-expressed with *SHH* at the ventral midline, we first asked whether BMP perturbations affect ventral midbrain cell-fate specification by modulating SHH (see Fig. S2A in the supplementary material) (Arkell and Beddington, 1997; Liem et al., 1997). Despite significant pSMAD1/5/8 reduction, BMP blockade between HH4-HH11 did not alter ventral cell-fate specification in E3-5 midbrains (Fig. 2D,E; see Fig. S2B-E″ in the supplementary material). However, noggin and dnBMPR1A manipulations at these stages induced multiple hinge-like invaginations and profoundly altered midbrain shape (Fig. 2F-H; see also Fig. 3 and Fig. 4I; see Fig. S3 in the supplementary material).

BMP blockade is necessary and sufficient for MHP formation

Given the ability of BMP blockade to elicit hinge-like invaginations and the low levels of pSMAD1/5/8 expression at the MHP, we asked whether BMP signaling could regulate endogenous MHP formation (Fig. 1D-H; Fig. 2F-H). Focal EGFP micro-electroporations at HH4-6 resulted in morphologically normal midbrain neural plates with proper MHP formation at HH7 and neural tube closure at HH10-11 (Fig. 3A-C; Table 1). By contrast, both noggin and dnBMPR1A electroporations resulted in a dramatic exaggeration of the endogenous MHP and in the ectopic induction of HPs in SOX2$^+$ midbrain neural plate (Fig. 3D-F; see Fig. S3A-E in the supplementary material; data not shown). The neural tube failed to close in BMP blockade experiments (n=9/11 embryos), most likely owing to the increased apicobasal thickening of the neural plate (compare Fig. 3A with 3D; Fig. 4I; Table 1) (Fraser, 1954).

Considerable controversy exists with regard to the requirement for MHP formation in neural tube closure (Copp et al., 2003; Smith and Schoenwolf, 1997). Strikingly, overexpression of caBMPR1A at the ventral midline during neural plate stages prevented MHP formation, flattening the ventral midline (Fig. 3G,H). Compared with controls (n=1/8), early midline electroporations of caBMPR1A, which prevented MHP formation, also consistently prevented the neural folds from elevating and drawing together so that they were unable to fuse across the dorsal midline (n=8/12; Fig. 3H,I, arrowheads; Table 1). Together, these results suggest that MHP formation is required for midbrain neural plate closure and that BMP blockade is necessary and sufficient for its induction.

Is MHP formation a cell-autonomous effect of BMP blockade?

The idiosyncratic inheritance of electroporated plasmids during cell division makes a determination of cell autonomy difficult. This problem is compounded by a variable, promoter-dependent shutdown of gene expression, often after a clear phenotype has been produced. Therefore, to determine whether the effects of BMP blockade were cell-autonomous, we examined embryos focally electroporated with dnBMPR1A-IRES-EGFP and collected 3 hours later. At this time, strong EGFP expression is detected and cell cycle duration (7-12 hours) is not a significant confounding factor

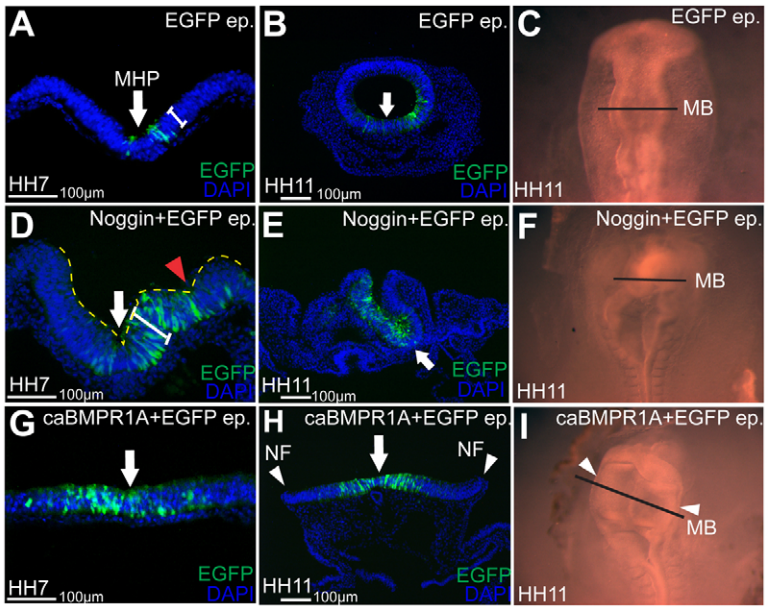

Fig. 3. BMP blockade is necessary and sufficient for MHP formation. Transverse sections of the chick midbrain (MB) (A,B,D,E,G,H) and whole embryos (C,F,I; top-down view; black lines indicate the level of sections in B,E,H). (**A-C**) EGFP electroporations at HH5 displaying a normally contoured MHP at HH7 and HH11 (arrows, A,B) and a correctly closed neural tube at HH11 (B,C). (**D-F**) Noggin overexpression at HH5 exaggerates the endogenous MHP (arrow in D,E) and induces ectopic HPs in lateral neural plate (red arrowhead, D). (**G-I**) Targeted midline caBMPR1A overexpression at HH5 abolishes the MHP (arrow, G) at HH7, and prevents the neural folds (arrowheads, H,I) from fusing at HH11.

(see Fig. S3D,E in the supplementary material; data not shown) (Schoenwolf, 1985; Smith and Schoenwolf, 1987). These dnBMPR1A manipulations clearly demonstrate that HP formation is a non-cell-autonomous event, involving BMP attenuation in some but not all cells of the HP.

BMP blockade can induce cell behaviors associated with MHP formation

MHP formation is associated with characteristic cell behaviors, such as basal nuclear migration, apical constriction and apicobasal shortening (Colas and Schoenwolf, 2001). We therefore asked whether such cell behaviors were induced in the HH7 neural plate by BMP blockade at HH4-6.

Apical constriction

A majority of cells at the endogenous MHP display constricted apical surfaces containing condensed apical actin (Fig. 4A,B) (Colas and Schoenwolf, 2001). To determine whether BMP blockade induced apical constriction, we compared the cellular apical- to widest-width (aw:ww) ratio in control and Noggin-electroporated cells stained with the apical marker PAR3 (see Materials and methods) (Lee et al., 2007). Compared with controls, noggin-electroporated cells displayed a 33.3% reduction in the aw:ww ratio, suggesting that apical constriction occurred in response to BMP blockade (Fig. 4C-E).

Basal migration of nuclei

In the wild-type MHP, nuclei spend more time at basal locations compared with those in the lateral neural plate (Fig. 4A,B) (Smith and Schoenwolf, 1997). We therefore asked whether BMP attenuation plays a role in inducing basal nuclear migration at ectopic hinges. Compared with DAPI- and PAR3-stained controls, noggin-electroporated nuclei occurred at more basal locations (8.15 μm versus 18.15 μm from the apical surface), reproducing the phenotype seen at the endogenous MHP (Fig. 4A,B,F-H and Fig. 2G, red arrowhead). Such increased basal nuclear migration (which results in greater apical constriction) also provides an explanation for the deeper MHP groove following noggin misexpression (Fig. 3D,E).

Apicobasal length

During neurulation, apicobasal shortening occurs at the MHP, while the neurectoderm lateral to the MHP undergoes apicobasal thickening (Colas and Schoenwolf, 2001). However, compared with controls, midbrain progenitors electroporated with noggin at HH4-6 rapidly increased their length by 45% by HH7 (Fig. 4I; compare the apicobasal thickness of sections in Fig. 4F with 4G and Fig. 3A with 3D; see Fig. 5C,D for individual cell spans). Together, these data suggest that BMP blockade is sufficient for apical constriction and basal nuclear migration, but not for apicobasal shortening. Interestingly, despite the inability of noggin to induce apicobasal shortening, it is sufficient to elicit ectopic HPs in the midbrain.

BMP signaling regulates epithelial apicobasal polarity

The above data show that BMP signaling regulates apicobasal cell behaviors associated with MHP formation. We therefore asked whether BMP signaling might affect MHP formation by interacting with the apicobasal polarity pathway. The apicobasal polarization of epithelial cells depends upon antagonistic interactions between basolateral [e.g. Lethal giant larva (LGL)-Scribble-Discs large] and apical [PAR3-PAR6-atypical protein kinase C (aPKC)] polarity protein complexes associated with tight and adherens junctions (Margolis and Borg, 2005). As a result, apical and basolateral proteins do not overlap in mature epithelia, although their expression can overlap in ‘morphogenetically active’ or immature epithelia (Ewald et al., 2008; Margolis and Borg, 2005; Suzuki et al., 2009).

To confirm the presence of fully polarized cells, we combined PAR3 or ZO1 immunohistochemistry with low-level LGL-GFP (1 μg/μl) misexpression at HH7-11 to visualize the apical and basolateral compartments at E3 (Dollar et al., 2005). Although cytoplasmic LGL-GFP was also present, it did not interfere with our ability to visualize polarized progenitors, which displayed fully segregated apical and basolateral compartments at E3 (see Fig. S6A,C,E in the supplementary material) (Betschinger et al., 2003). Thus, low-level LGL-GFP electroporations do not affect apicobasal polarity.

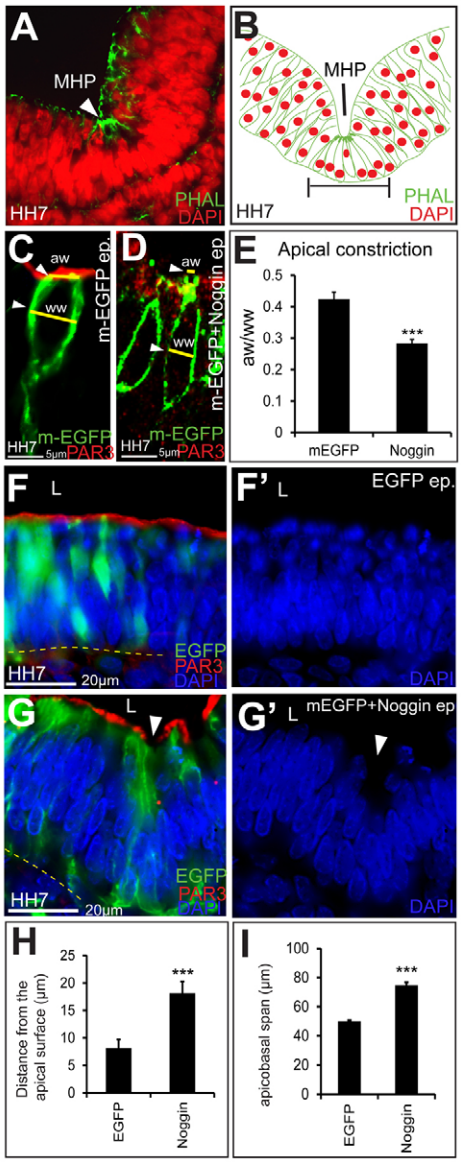

Fig. 4. BMP signaling regulates apicobasal cell behaviors associated with MHP formation. (**A**) DAPI (red) and phalloidin (green) stained chick neural plate demonstrating condensed phalloidin (apical constriction) and basal nuclear migration in most, but not all, cells at the MHP. (**B**) Schematic representation of A. (**C-E**) Compared with controls (C), noggin-electroporated cells (D) display reduced apical width:widest cell width (aw:ww) ratios. Yellow lines and arrowheads indicate where aw and ww measurements were made. (E) Quantitation of C,D. The aw:ww ratios in control cells (0.42; *n*=33 cells/6 brains) and noggin-electroporated cells (0.28; *n*=41cells/7 brains) are significantly different (***, $P=2.59\times10^{-8}$). (**F**,**F′**) EGFP electroporations displaying the smooth apical (PAR3$^+$) contour of the lateral midbrain and the normal distribution of DAPI-stained nuclei. Note that the density of DAPI staining is lower apically in wild-type brains than elsewhere. (**G**,**G′**) Noggin-induced ectopic hinge in lateral midbrain (arrowhead) displays apical constriction, basally located nuclei and reduced apical PAR3. F′ and G′ show the DAPI channel alone. (**H**) Quantitation of basal migration. The distances from the apical surface for control cells (8.15 μm; *n*=56 cells/5 brains) and noggin-treated cells (18.14 μm; *n*=78 cells/6 brains) are significantly different (***, $P=3.15\times10^{-7}$). (**I**) Compared with EGFP-electroporated controls (49.2 μm; *n*=17 cells/5 brains), noggin-electroporated cells (72.52 μm; 42 cells/10 brains) display increased apicobasal spans (***, $P=1.05\times10^{-12}$). Error bars indicate s.e.m.

Table 1. The effects of BMP signaling on neural tube closure

Treatment	Unaffected	NTD	Total
EGFP	7	1	8
Noggin	2	9	11
caBMPR1A	4	8	12

Phenotypes of EGFP, noggin and caBMPR1A misexpressing midbrains electroporated at HH5 and examined at HH11 for neural tube closure defects (NTDs).

By contrast, low-level LGL-GFP electroporations encompassing a broad swath of the neural plate at HH4-6 displayed many partially polarized cells (with apical LGL or LGL-PAR3 overlap) at the MHP (*n*=11/16 electroporated), compared with only a few in lateral midbrain (*n*=3/19 electroporated; Fig. 5A-A″,B). Thus, the frequency of partially polarized cells was highest at the MHP and lowest in lateral neural plate, where low and high levels of BMP signaling were respectively noted.

We next asked whether partially polarized cells could be induced by BMP blockade in lateral neural plate (Fig. 5A-B). Compared with low-level LGL-GFP electroporations in lateral neural plate, where only 15.8% cells were partially polarized (*n*=3/19), 62.7% cells co-electroporated with noggin and low-level LGL-GFP were partially polarized (*n*=37/59; Fig. 5B-E″). Since HP formation depends upon dynamic, cell cycle-dependent, graded BMP signaling, such cells variably displayed combinations of polarity phenotypes including apical LGL-GFP, reduced apical PAR3, ZO1 and N-CAD, LGL-PAR3 overlap, apical constriction and basal nuclear migration (Fig. 5C-E″; see Fig. S4A-C‴ in the supplementary material). Together, these data suggest that BMP signaling regulates apicobasal polarity in the neurectoderm.

BMP blockade results in the endocytosis of apical proteins

Despite the apical loss of PAR3, western blot analyses demonstrated that the total levels of PAR3 protein did not differ between control and noggin-electroporated brains (Fig. 5F). We noted that noggin-electroporated cells frequently displayed PAR3$^+$ ZO1$^+$ N-CAD$^+$ cytoplasmic puncta not seen in controls (Fig. 5D,I; see Fig. S4A-C‴ in the supplementary material). We therefore hypothesized that the apical loss of PAR3 might be due to the endocytosis-mediated removal of apical membranes, serving as a partial cause of apical constriction.

As in gastrulating *Xenopus* bottle cells (Lee and Harland, 2010), control neural plates displayed little expression of the early endosomal markers EEA1 or RAB5, suggesting that these organelles turn over rapidly (Fig. 5A,G-I‴; data not shown). The only exception to this general observation was the MHP, where EEA1$^+$ puncta could clearly be seen (Fig. 5A,G,G′, arrowheads). This phenotype was reproduced in noggin-electroporated brains, which displayed an increase in PAR3$^+$ EEA1$^+$ puncta, demonstrating that a proportion of apical PAR3 had been shunted into endocytic vesicles (Fig. 5H-I‴; 1 punctum/72 cells/3 brains for control cells versus 10 puncta/57 cells/3 brains for noggin-electroporated brains). These results were confirmed by co-electroporations of noggin with RAB5-mCherry, which also demonstrated increased numbers of PAR3$^+$ RAB5-mCherry$^+$ cytoplasmic puncta compared with control brains (see Fig. S4D-E‴ in the supplementary material). Thus, these results implicate BMP blockade-mediated endocytosis of apical proteins as a potential partial cause of apical constriction.

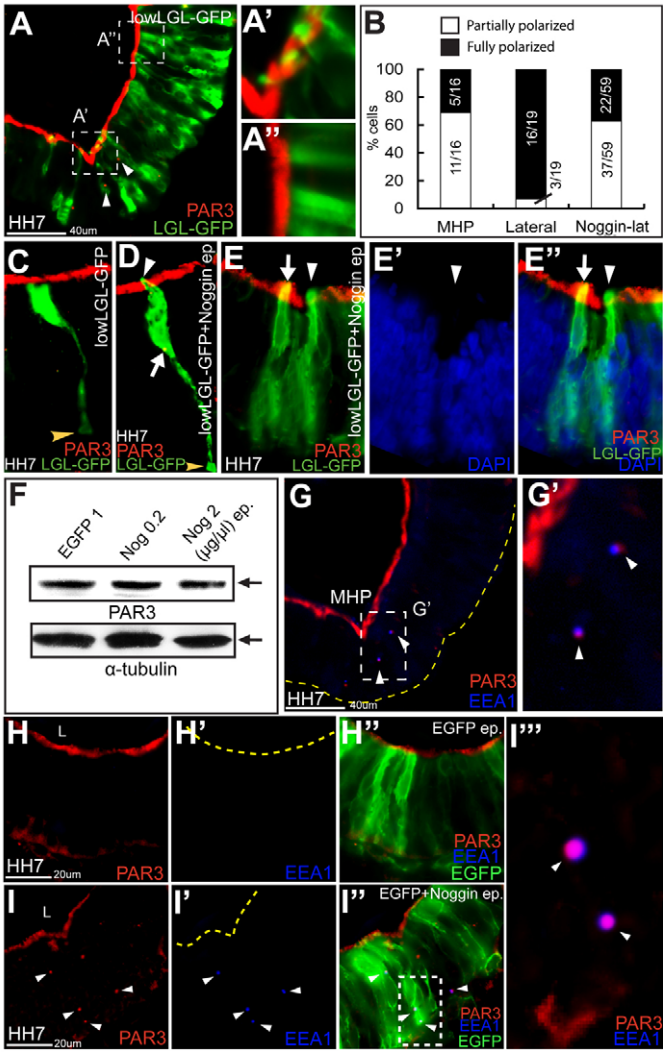

Fig. 5. BMP signaling regulates epithelial apicobasal polarity. (**A-A″**) Control chick brain electroporated at HH4-6 with low-level LGL-GFP displays semi-polarized cells, with apical LGL-GFP at the MHP (A,A′). By contrast, a clear segregation between apical (PAR3$^+$) and basolateral (LGL$^+$) compartments is evident in the lateral neural plate of the same embryo (A,A″). A′,A″ show magnified views of the boxed areas in A. Arrowheads, identify PAR3$^+$ puncta, labeled with the endosomol marker EEA1 in G,G′. (**B**) Ratio of polarized to partially polarized cells at the MHP and lateral neural plate in low-level LGL-GFP controls (left and middle) and in noggin-electroporated lateral neural plate (right). Percentage of partially polarized cells at: the control MHP, 68.8% (*n*=11/16 electroporated cells); control lateral neural plate, 15.8% (*n*=3/19 electroporated cells); noggin-electroporated lateral neural plate, 62.7% (*n*=37/59 electroporated). Control MHP versus lateral neural plate, *P*=0.00223; control versus noggin-electroporated lateral neural plate, *P*=0.00147. (**C**) Control HH4-6 LGL-GFP electroporations showing complete segregation of the apical and basolateral compartments in an apical nucleus in the lateral midbrain. Orange arrowhead at the bottom (C,D) indicates the basal foot of the cell. (**D-E″**) Noggin plus low-level LGL-GFP electroporations display variable combinations of ectopic apical LGL-GFP (arrowhead, D,E), reduced apical PAR3 (arrowheads, D,E), PAR3-LGL-GFP overlap (arrow, E,E″), cytoplasmic PAR3 (arrow in D; see also H-I‴), apical constriction (arrowheads, D,E-E″; arrow, E,E″), basal nuclear migration (E-E″) and ectopic HP formation (E-E″). E″ is a merge of E,E′. (**F**) Western blots showing that PAR3 levels (top row) do not differ in control or noggin-electroporated E3 whole cell lysates. Bottom row shows the loading control. (**G**,**G′**) HH7 neural plate electroporated at HH4-6 with low-level LGL-GFP displaying PAR3$^+$ EEA1$^+$ puncta (arrowheads) at the MHP, but not lateral neural plate. The boxed area in G is shown at high magnification in G′. G shows the same micrograph as A but with EEA1 staining (blue). Arrowheads in A and G,G′ point to the same PAR3$^+$ puncta. (**H-I‴**) Low-magnification (H-I″) and high-magnification (I‴) images demonstrating that, compared with controls (H-H″), noggin-electroporated embryos display increased PAR3$^+$ cytoplasmic puncta, which colocalize with EEA1$^+$ endosomes (arrowheads, I-I‴). Number of PAR3$^+$ EEA1$^+$ puncta in control cells, 1/72 cells/3 brains; PAR3$^+$ EEA1$^+$ puncta in noggin plus EGFP electroporated cells, 10/57 cells/3 brains.

Ectopic apical LGL is sufficient to induce MHP formation

The above results suggest that noggin misexpression mimics the events at the endogenous MHP by modulating apicobasal cell polarity. We therefore asked to what extent would direct manipulations of apicobasal polarity proteins (e.g. LGL-GFP) account for the HP-associated effects of BMP blockade. Unlike low-level LGL-GFP misexpression, high-level LGL-GFP (3-5 µg/µl) electroporations at HH4-11 resulted in aberrant apical LGL-GFP expression and in ectopic HP induction in SOX2$^+$ lateral neural plate (Fig. 6A,B,F; see Fig. S5A-A‴ in the supplementary material). As with BMP blockade, such ectopic HPs also variably displayed combinations of apical constriction, basal nuclear migration, loss of apical PAR3 and increased PAR3 endocytosis into EEA1$^+$ endosomes (Fig. 6C-G‴). Furthermore, LGL-GFP electroporations followed by short-term survivals (3 hours) induced HP formation in a non-cell-autonomous manner, as did dnBMPR1A manipulations (Fig. 6B; see Fig. S3D,E in the supplementary material). We conclude that BMP blockade targets LGL to the apical compartment. Apical LGL, in turn, is sufficient to account for the cellular and morphogenetic effects of BMP blockade on MHP formation.

The BMP signaling cascade biochemically interacts with members of the apicobasal polarity pathway

Given the ability of BMP attenuation to alter the apicobasal localization of polarity proteins, we asked whether the BMP signaling cascade biochemically interacts with the apicobasal polarity pathway. Whole cell lysates were prepared from HH9-11 wild-type midbrains or electroporated regions of E3 midbrains to obtain sufficient quantities of tissue for analyses. Since this tissue was collected after the neural tube had closed, we first established that ectopic HPs and polarity changes induced by noggin at neural plate stages or later (E1-3) were indistinguishable from each other and resembled the endogenous MHP based on multiple criteria (see Fig. S6 in the supplementary material). These included HP induction, basal nuclear migration, apical constriction, ectopic apical LGL-GFP, downregulation of apical PAR3 and the presence of cytoplasmic PAR3$^+$ EEA1$^+$ puncta (Fig. 2F-G′; see Fig. S6 in the supplementary material; data not shown).

Co-immunoprecipitation experiments in wild-type whole cell lysates demonstrated biochemical interactions between pSMAD1,5,8 and members of the apical polarity complex (PAR3, PAR6, aPKC; Fig. 7A-C). Low-level (1 µg/µl) PAR3-GFP electroporations followed by pSMAD1/5/8 immunohistochemistry

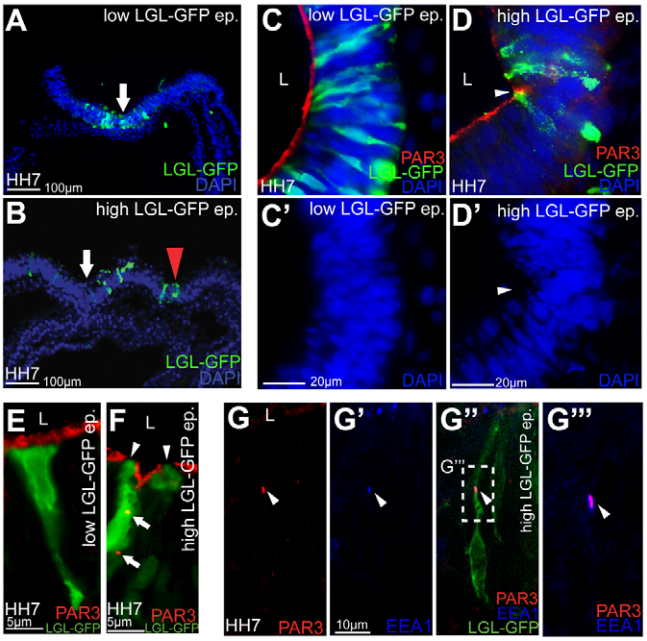

Fig. 6. LGL-GFP misexpression is sufficient to induce ectopic HP formation. (**A**,**B**) Unlike control or low-level LGL-GFP (A), high-level (3 μg/μl) LGL-GFP misexpression at HH5 is sufficient to induce ectopic HPs by HH7 (red arrowhead, B). (**C-D'**) Control (C,C′) and high-level LGL-GFP misexpression (D,D′), which demonstrates apical LGL, loss of apical PAR3 and basal nuclear migration. C′ and D′ show the DAPI channel alone. (**E**,**F**) Low-level (E) and high-level (F) LGL-GFP electroporations demonstrating apical LGL-GFP and apical constriction in the latter (F, arrowheads). (**G-G‴**) Ectopic cytoplasmic PAR3^{+} EEA1^{+} puncta in cells electroporated with high levels of LGL-GFP. (G,G′) Single channels; (G″) merge of G,G′ and LGL-GFP; (G‴) merge of G,G′ showing the boxed area in G″.

further confirmed the colocalization of pSMAD1/5/8 and PAR3 (Fig. 7D-D″). Thus, pSMAD1/5/8 proteins biochemically interact with the PAR3-aPKC-PAR6 complex that is normally associated with the tight junction (Fig. 7A-D).

A severe reduction in PAR3-pSMAD1/5/8 interactions occurred in noggin-electroporated lysates, but not in EGFP-electroporated lysates (Fig. 7E). This reduced interaction occurred in the absence of a reduction in PAR3, SMAD1 or SMAD5 protein levels following noggin electroporations (Fig. 2C; Fig. 5F; Fig. 7E). Since no interactions occurred between SMAD1 and PAR3 in wild-type lysates (data not shown) and the SMAD8 antibody did not work in our hands, we focused our analyses on PAR3-SMAD5 interactions and found that the association of pSMAD5 with the apical polarity complex was also BMP dependent (Fig. 7F). Together, these data suggest that a PAR3-PAR6-aPKC complex associates with pSMAD5 at the tight junction in a BMP-dependent manner.

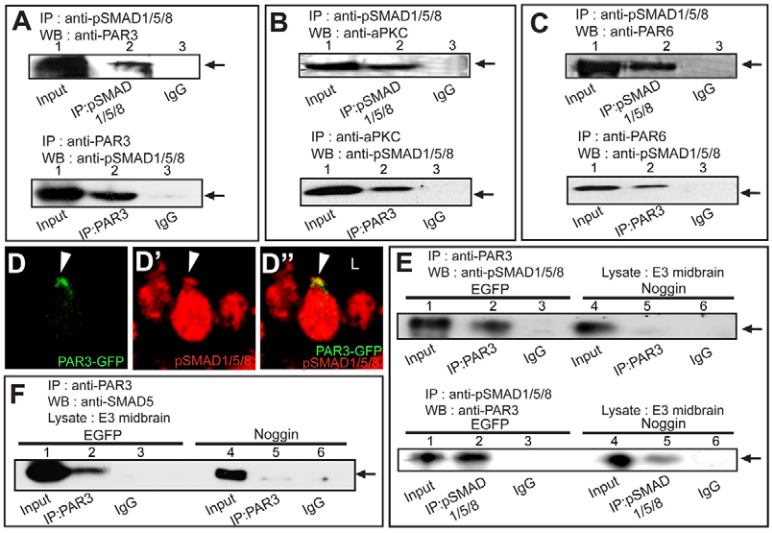

Fig. 7. pSMAD1/5/8 biochemically associates with the apicobasal polarity protein complex (PAR3-PAR6-aPKC) at apical junctions. (**A**) (Top) Biochemical interactions between pSMAD1/5/8 and PAR3 in whole cell lysates immunoprecipitated with PAR3 and immunoblotted with pSMAD1/5/8 antibody (lane 2). (Bottom) pSMAD1/5/8 and PAR3 interactions demonstrated by reversing pSMAD1/5/8 and PAR3 antibodies (lane 2). (**B**,**C**) pSMAD1/5/8 interacts with aPKC (B, lane 2, top and bottom) and PAR6 (C, lane 2, top and bottom). Details as in A. (**D-D″**) PAR3-GFP electroporation and pSMAD1/5/8 immunostaining demonstrating PAR3 and pSMAD1/5/8 (red) colocalization at the apical surface (arrowhead). (**E**) Compared with EGFP controls, biochemical interactions between pSMAD1/5/8 and PAR3 are reduced in noggin-electroporated lysates: compare lanes 2 and 5, top row (IP: PAR3; WB: pSMAD1/5/8) and lanes 2 and 5, bottom row (IP: pSMAD1/5/8; WB: PAR3). (**F**) Immunoprecipitation with PAR3 and western blotting with a SMAD5 antibody (which recognizes both the phosphorylated and non-phosphorylated forms). Note that the interactions between PAR3 and SMAD5 seen in EGFP-electroporated embryos (lane 2) are greatly reduced upon noggin electroporation (lane 5). IP, immunoprecipitation; WB, western blot.

DISCUSSION

Noggin or dnBMPR1A overexpression at neural plate stages exaggerates the endogenous MHP, whereas caBMPR1A misexpression abolishes it. This has led us to conclude that noggin plays a crucial role in MHP formation, despite the inability of noggin to induce ventral midline cell fates and apicobasal shortening. Noggin has also been implicated in DLHP formation in the mouse, although the cellular mechanisms regulated by noggin at the DLHP have not yet been examined (Stottmann et al., 2006; Ybot-Gonzalez et al., 2007). The shifting position of the DLHP during neural tube closure, the absence of DLHP-specific molecular markers and the difficulty of identifying a DLHP by morphology in sections of the open neural plate have prevented us from exploring DLHP induction mechanisms in this study. Our analyses are therefore confined to MHP formation and the general mechanisms involved in HP formation (e.g. apical constriction and basal nuclear migration).

Graded BMP signaling, the dynamic regulation of polarity and neural tube closure

In this study, we show that the dynamic modulation of epithelial polarity by BMP signaling plays a crucial role in neural tube closure. In vertebrate epithelia, the LGL-Discs large-Scribble protein complex is associated with the inner leaflet of the basolateral cell membrane, whereas the PAR3-PAR6-aPKC complex localizes at apical junctions (Afonso and Henrique, 2006; Hurd and Margolis, 2005; Musch et al., 2002; Yamanaka et al., 2006). LGL is phosphorylated by aPKC and competes with PAR3 for association with the aPKC-PAR6 complex (Yamanaka et al., 2006). Antagonistic interactions between these apical and basolateral protein complexes have been shown to be important for apical junctional integrity in flies and vertebrates (Aaku-Saraste et al., 1996; Chalmers et al., 2005).

Here, we show that canonical BMP blockade alters apicobasal polarity by disrupting apical junctions. As a result, LGL is targeted to the apical compartment and junctional proteins are targeted away from the apical compartment into $EEA1^{+}$ $RAB5^{+}$ endosomes, without significant alterations in the total levels of PAR3 or SMAD proteins. Direct apical LGL misexpression in turn is sufficient to induce ectopic HPs associated with apical constriction, basal nuclear migration and PAR3 endocytosis.

How BMP signaling maintains the apical localization of PAR3 and prevents the apical localization of LGL is currently unknown, but a model supported by our data is proposed in Fig. 8. The PAR3-PAR6-aPKC protein complex associates with apical junctions in epithelial cells (Margolis and Borg, 2005). Since PAR3, PAR6 and aPKC complex with pSMAD5/8 in a BMP-dependent manner, pSMAD5/8 must also be associated with apical junctions when the cell receives BMP signaling (Fig. 8A) (Warner et al., 2003). In the absence of canonical BMP signaling, the phosphorylation of SMAD proteins is severely attenuated, reducing interactions with the apical polarity complex (Fig. 8B). We propose that, in the absence of association with pSMAD5/8, PAR3 cannot remain associated with the apical protein complex, resulting in its endocytic removal to the cytoplasm and the apical expression of LGL (Fig. 8B) (Lee and Harland, 2010).

It is worth noting that high, intermediate and low BMP states can occur in the same cell and can dynamically govern its polarity depending on its cell cycle state (Fig. 8A,B). This might account for the variability in the polarity phenotypes seen following BMP manipulations in the neural plate (Fig. 5C-E‴). Further dynamic modulation could emerge if a handful of BMP-modulated neural progenitors were to influence the behaviors of their neighbors via modified apical junctions, producing multicellular, non-autonomous and mosaic events such as HP formation (Colas and Schoenwolf, 2001). In this scenario, not all cells participating in hinge formation would be required to display altered polarity (e.g. Fig. 5A,E, Fig. 6F) at any given time point, although many would do so in order to generate the required mechanical forces. This scenario is compatible with our observations of cell cycle-dependent and mosaic pSMAD1/5/8 expression in the neural plate and the presence of a combination of polarized and partially polarized cells at the endogenous MHP (Colas and Schoenwolf, 2001).

We propose that the mosaic and cell cycle-dependent nature of BMP activity, superimposed on its mediolateral gradient, assures that BMP modulation can dynamically alter the polarity of targeted cells while maintaining epithelial polarity in their neighbors. This dynamic modulation of polarity in turn provides the neural plate with the flexibility to bend and shape into a neural tube while maintaining overall epithelial integrity (Bryant and Mostov, 2008). Such partially polarized cells have also been noted in other morphogenetically active epithelia undergoing organogenesis (Ewald et al., 2008; Suzuki et al., 2009; Yang et al., 2009).

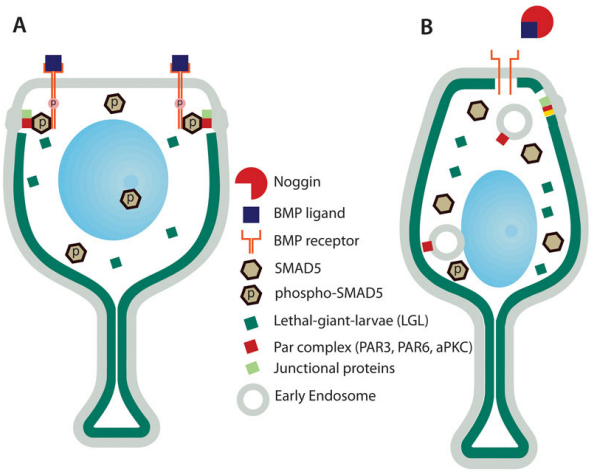

Fig. 8. A model for the cellular role of BMP signaling in regulating apicobasal polarity. (**A**) A neural plate cell receiving BMP signaling. BMP binding to its receptors phosphorylates pSMAD1/5/8, which associates with the PAR3-PAR6-aPKC complex at the tight junction. The PAR complex is stabilized and LGL is restricted to the basolateral compartment and cytoplasm. (**B**) A cell experiencing BMP attenuation. Owing to reduced SMAD5/8 phosphorylation, the PAR complex becomes unstable and disrupts the tight junction. This permits the apical incursion of LGL, PAR3 endocytosis and apical constriction. Note that the same cell can shuttle between states A and B in a cell cycle-dependent manner. Blue oval, nucleus.

Acknowledgements

We thank Drs J. Morgan and R. Raghavan for help with co-immunoprecipitation; Drs Y. Wakamatsu, C. Ragsdale, L. Niswander, D. Duprez, S. Sokol and M. Takeichi, B. Houston, P. Brickell, D. Wu, C. Tabin, A. Graham, J. Cooke, C. Goridis, M. Goulding, G. Martin, A. McMahon and A. Ruegels for reagents; J. Gross for use of his confocal microscope; and J. Gross, D. Stein, C. Ragsdale and T. Shimogori for helpful discussions. This work was supported by an NIH-NINDS grant to S.A. Deposited in PMC for release after 12 months.

Competing interests statement

The authors declare no competing financial interests.

Supplementary material

Supplementary material for this article is available at
http://dev.biologists.org/lookup/suppl/doi:10.1242/dev.058602/-/DC1

References

Aaku-Saraste, E., Hellwig, A. and Huttner, W. B. (1996). Loss of occludin and functional tight junctions, but not ZO-1, during neural tube closure-remodeling of the neuroepithelium prior to neurogenesis. *Dev. Biol.* **180**, 664-679.

Afonso, C. and Henrique, D. (2006). PAR3 acts as a molecular organizer to define the apical domain of chick neuroepithelial cells. *J. Cell Sci.* **119**, 4293-4304.

Agarwala, S. and Ragsdale, C. W. (2002). A role for midbrain arcs in nucleogenesis. *Development* **129**, 5779-5788.

Agarwala, S., Sanders, T. A. and Ragsdale, C. W. (2001). Sonic hedgehog control of size and shape in midbrain pattern formation. *Science* **291**, 2147-2150.

Andrew, D. J. and Ewald, A. J. (2010). Morphogenesis of epithelial tubes: insights into tube formation, elongation, and elaboration. *Dev. Biol.* **341**, 34-55.

Arkell, R. and Beddington, R. S. (1997). BMP-7 influences pattern and growth of the developing hindbrain of mouse embryos. *Development* **124**, 1-12.

Attisano, L. and Wrana, J. L. (2002). Signal transduction by the TGF-beta superfamily. *Science* **296**, 1646-1647.

Betschinger, J., Mechtler, K. and Knoblich, J. A. (2003). The Par complex directs asymmetric cell division by phosphorylating the cytoskeletal protein Lgl. *Nature* **422**, 326-330.

Brouns, M. R., Matheson, S. F., Hu, K. Q., Delalle, I., Caviness, V. S., Silver, J., Bronson, R. T. and Settleman, J. (2000). The adhesion signaling molecule p190 RhoGAP is required for morphogenetic processes in neural development. *Development* **127**, 4891-4903.

Bryant, D. M. and Mostov, K. E. (2008). From cells to organs: building polarized tissue. *Nat. Rev. Mol. Cell Biol.* **9**, 887-901.

Bucci, C., Parton, R. G., Mather, I. H., Stunnenberg, H., Simons, K., Hoflack, B. and Zerial, M. (1992). The small GTPase rab5 functions as a regulatory factor in the early endocytic pathway. *Cell* **70**, 715-728.

Chalmers, A. D., Pambos, M., Mason, J., Lang, S., Wylie, C. and Papalopulu, N. (2005). aPKC, Crumbs3 and Lgl2 control apicobasal polarity in early vertebrate development. *Development* **132**, 977-986.

Colas, J. F. and Schoenwolf, G. C. (2001). Towards a cellular and molecular understanding of neurulation. *Dev. Dyn.* **221**, 117-145.

Copp, A. J., Greene, N. D. and Murdoch, J. N. (2003). The genetic basis of mammalian neurulation. *Nat. Rev. Genet.* **4**, 784-793.

Davidson, L. A. and Keller, R. E. (1999). Neural tube closure in Xenopus laevis involves medial migration, directed protrusive activity, cell intercalation and convergent extension. *Development* **126**, 4547-4556.

Dollar, G. L., Weber, U., Mlodzik, M. and Sokol, S. Y. (2005). Regulation of lethal giant larvae by Dishevelled. *Nature* **437**, 1376-1380.

Ewald, A. J., Brenot, A., Duong, M., Chan, B. S. and Werb, Z. (2008). Collective epithelial migration and cell rearrangements drive mammary branching morphogenesis. *Dev. Cell* **14**, 570-581.

Fraser, R. C. (1954). Studies on the hypoblast of the young chick embryo. *J. Exp. Zool.* **126**, 349-399.

Gibson, M. C. and Perrimon, N. (2005). Extrusion and death of DPP/BMP-compromised epithelial cells in the developing Drosophila wing. *Science* **307**, 1785-1789.

Haigo, S. L., Hildebrand, J. D., Harland, R. M. and Wallingford, J. B. (2003). Shroom induces apical constriction and is required for hingepoint formation during neural tube closure. *Curr. Biol.* **13**, 2125-2137.

Hamburger, V. and Hamilton, H. L. (1951). A series of normal stages in the development of the chick embryo. *J. Morphol.* **88**, 49-92.

Hurd, T. W. and Margolis, B. (2005). Pars and polarity: taking control of Rac. *Nat. Cell Biol.* **7**, 205-207.

Jacobson, A. G., Oster, G. F., Odell, G. M. and Cheng, L. Y. (1986). Neurulation and the cortical tractor model for epithelial folding. *J. Embryol. Exp. Morphol.* **96**, 19-49.

Johnson, A. D. and Krieg, P. A. (1994). pXeX, a vector for efficient expression of cloned sequences in Xenopus embryos. *Gene* **147**, 223-226.

Langman, J., Guerrant, R. L. and Freeman, B. G. (1966). Behavior of neuro-epithelial cells during closure of the neural tube. *J. Comp. Neurol.* **127**, 399-411.

Lee, C., Scherr, H. M. and Wallingford, J. B. (2007). Shroom family proteins regulate gamma-tubulin distribution and microtubule architecture during epithelial cell shape change. *Development* **134**, 1431-1441.

Lee, J. Y. and Harland, R. M. (2010). Endocytosis is required for efficient apical constriction during Xenopus gastrulation. *Curr. Biol.* **20**, 253-258.

Liem, K. F., Jr, Tremml, G. and Jessell, T. M. (1997). A role for the roof plate and its resident TGFbeta-related proteins in neuronal patterning in the dorsal spinal cord. *Cell* **91**, 127-138.

Liu, A. and Niswander, L. A. (2005). Bone morphogenetic protein signalling and vertebrate nervous system development. *Nat. Rev. Neurosci.* **6**, 945-954.

Margolis, B. and Borg, J. P. (2005). Apicobasal polarity complexes. *J. Cell Sci.* **118**, 5157-5159.

Massague, J. (2008). TGFbeta in cancer. *Cell* **134**, 215-230.

McMahon, J. A., Takada, S., Zimmerman, L. B., Fan, C. M., Harland, R. M. and McMahon, A. P. (1998). Noggin-mediated antagonism of BMP signaling is required for growth and patterning of the neural tube and somite. *Genes Dev.* **12**, 1438-1452.

Musch, A., Cohen, D., Yeaman, C., Nelson, W. J., Rodriguez-Boulan, E. and Brennwald, P. J. (2002). Mammalian homolog of Drosophila tumor suppressor lethal (2) giant larvae interacts with basolateral exocytic machinery in Madin-Darby canine kidney cells. *Mol. Biol. Cell* **13**, 158-168.

Nagele, R. G., Bush, K. T., Kosciuk, M. C., Hunter, E. T., Steinberg, A. B. and Lee, H. Y. (1989). Intrinsic and extrinsic factors collaborate to generate driving forces for neural tube formation in the chick: a study using morphometry and computerized three-dimensional reconstruction. *Brain Res. Dev. Brain Res.* **50**, 101-111.

Nishimura, T. and Takeichi, M. (2008). Shroom3-mediated recruitment of Rho kinases to the apical cell junctions regulates epithelial and neuroepithelial planar remodeling. *Development* **135**, 1493-1502.

Ozdamar, B., Bose, R., Barrios-Rodiles, M., Wang, H. R., Zhang, Y. and Wrana, J. L. (2005). Regulation of the polarity protein Par6 by TGFbeta receptors controls epithelial cell plasticity. *Science* **307**, 1603-1609.

Sai, X. and Ladher, R. K. (2008). FGF signaling regulates cytoskeletal remodeling during epithelial morphogenesis. *Curr. Biol.* **18**, 976-981.

Sauer, L. (1935). Mitosis in the neural tube. *J. Comp. Neurol.* **62**, 377-397.

Schoenwolf, G. C. (1985). Shaping and bending of the avian neuroepithelium: morphometric analyses. *Dev. Biol.* **109**, 127-139.

Shen, J. and Dahmann, C. (2005). Extrusion of cells with inappropriate Dpp signaling from Drosophila wing disc epithelia. *Science* **307**, 1789-1790.

Shoval, I., Ludwig, A. and Kalcheim, C. (2007). Antagonistic roles of full-length N-cadherin and its soluble BMP cleavage product in neural crest delamination. *Development* **134**, 491-501.

Smith, J. L. and Schoenwolf, G. C. (1987). Cell cycle and neuroepithelial cell shape during bending of the chick neural plate. *Anat. Rec.* **218**, 196-206.

Smith, J. L. and Schoenwolf, G. C. (1997). Neurulation: coming to closure. *Trends Neurosci.* **20**, 510-517.

Stottmann, R. W., Berrong, M., Matta, K., Choi, M. and Klingensmith, J. (2006). The BMP antagonist Noggin promotes cranial and spinal neurulation by distinct mechanisms. *Dev. Biol.* **295**, 647-663.

Suzuki, T., Elias, B. C., Seth, A., Shen, L., Turner, J. R., Giorgianni, F., Desiderio, D., Guntaka, R. and Rao, R. (2009). PKC eta regulates occludin phosphorylation and epithelial tight junction integrity. *Proc. Natl. Acad. Sci. USA* **106**, 61-66.

Swartz, M., Eberhart, J., Mastick, G. S. and Krull, C. E. (2001). Sparking new frontiers: using in vivo electroporation for genetic manipulations. *Dev. Biol.* **233**, 13-21.

Umans, L., Vermeire, L., Francis, A., Chang, H., Huylebroeck, D. and Zwijsen, A. (2003). Generation of a floxed allele of Smad5 for cre-mediated conditional knockout in the mouse. *Genesis* **37**, 5-11.

van Straaten, H. W., Sieben, I. and Hekking, J. W. (2002). Multistep role for actin in initial closure of the mesencephalic neural groove in the chick embryo. *Dev. Dyn.* **224**, 103-108.

von der Hardt, S., Bakkers, J., Inbal, A., Carvalho, L., Solnica-Krezel, L., Heisenberg, C. P. and Hammerschmidt, M. (2007). The Bmp gradient of the zebrafish gastrula guides migrating lateral cells by regulating cell-cell adhesion. *Curr. Biol.* **17**, 475-487.

Warner, D. R., Pisano, M. M., Roberts, E. A. and Greene, R. M. (2003). Identification of three novel Smad binding proteins involved in cell polarity. *FEBS Lett.* **539**, 167-173.

Yamanaka, T., Horikoshi, Y., Izumi, N., Suzuki, A., Mizuno, K. and Ohno, S. (2006). Lgl mediates apical domain disassembly by suppressing the PAR-3-aPKC-PAR-6 complex to orient apical membrane polarity. *J. Cell Sci.* **119**, 2107-2118.

Yang, X., Zou, J., Hyde, D. R., Davidson, L. A. and Wei, X. (2009). Stepwise maturation of apicobasal polarity of the neuroepithelium is essential for vertebrate neurulation. *J. Neurosci.* **29**, 11426-11440.

Ybot-Gonzalez, P., Cogram, P., Gerrelli, D. and Copp, A. J. (2002). Sonic hedgehog and the molecular regulation of mouse neural tube closure. *Development* **129**, 2507-2517.

Ybot-Gonzalez, P., Gaston-Massuet, C., Girdler, G., Klingensmith, J., Arkell, R., Greene, N. D. and Copp, A. J. (2007). Neural plate morphogenesis during mouse neurulation is regulated by antagonism of Bmp signalling. *Development* **134**, 3203-3211.